GEMSTONES FROM VIGNA BARBERINI AT THE PALATINE HILL (ROME, ITALY)*

E. GLIOZZO

Department of Earth Sciences, University of Siena, Via Laterini 8, 53100 Siena, Italy

N. GRASSI

Istituto Nazionale di Fisica Nucleare, Via G. Sansone 1, 50019 Sesto Fiorentino, Firenze, Italy

P. BONANNI

Department of Physics, University of Florence and Istituto Nazionale di Fisica Nucleare, Via G. Sansone 1, 50019 Sesto Fiorentino, Firenze, Italy

C. MENEGHINI

Department of Physics, Roma Tre University, Rome, Italy

and M. A. TOMEI

Soprintendenza Archeologica di Roma, Direzione Palatino-Foro Romano, Rome, Italy

This study investigates 25 gemstones (23 intaglios and two undecorated cabochon, used between the third quarter of the first century AD *and the second century* AD*) found in the archaeological excavations performed at 'Vigna Barberini', in the north-east sector of the Palatine Hill in Rome. The analytical results obtained by means of SR-XRD, Raman microspectroscopy and PIXE measurements provided, in a totally non-destructive mode, unambiguous characterization of the gemstones. The collection from Vigna Barberini consists of two colourless chalcedonies, 11 carnelians, one sard, three Cr-bearing chalcedonies, two nicoli, two orange jaspers, one heliotrope, one almandine garnet, one peridote and one lapis lazuli. Given the lack of analytical data discriminating between different sources, the worldwide occurrence of all these gemstones makes it difficult to reconstruct preferential routes for their commercial trade. However, the methodological approach followed for this research should be of help for the identification of discrimination parameters for provenance investigation.*

KEYWORDS: GEMSTONE, SR-XRD, PIXE, VIGNA BARBERINI

INTRODUCTION

The investigations, conducted by the Soprintendenza Archeologica di Roma and the École Française de Rome (in the years 1985–98) at 'Vigna Barberini', in the north-east sector of the Palatine Hill in Rome (Villedieu 2001, 2007), brought to light a collection of 25 gemstones (23 intaglios and two undecorated cabochons), used between the third quarter of the first century AD and the second century AD. Indeed, the mineralogical and chemical composition of these gem-

stones was required in order to achieve an unambiguous characterization of these precious archaeological objects and to provide the basic information for the archaeological study itself. Hence, the characterization of the whole collection represented the aim of this research. Based on the results obtained, some further technological considerations were made.

A provenance investigation immediately seemed hopeless, when macroscopic analysis revealed that most of the gemstone collection was probably constituted by chalcedonies. Nevertheless, some attempts had previously been made and we took up the challenge. Unfortunately, the results did not allow us to provide meaningful archaeological reconstructions; the hypotheses we suggested were mainly based on archaeological and historical considerations, supported by a survey of geological resource availability in the Mediterranean area. Fortunately, the research achieved two important results from a methodological point of view. First, we tested an analytical protocol that provided an accurate gemstone characterization in a totally non-destructive and non-invasive way. Second, the attempts made to trace the gemstone origins clarified the limits and future perspectives of some techniques, providing useful insights for the future development of this field of study. After this necessary premise, it is important to briefly describe the state of the art of these studies; indeed, focusing only on those gemstones that will be considered in the present research.

Despite their importance, in terms of preciousness, aesthetic properties, mysterious virtues, commercial trade and social destination, gemstone studies remain still largely unaddressed. Comprehensive studies on garnets have been performed on those found in Paris (Farges 1998; Calligaro *et al.* 2002), in Belgium (Mathis *et al.* 2008) and in the United Kingdom (Bimson *et al.* 1982). A large database of garnet chemical composition (1290 garnets on 131 Merovingian artefacts found in France) was provided by Calligaro *et al.* (2006–7) for provenance investigations.

Extraction procedures, engraving techniques, uses and source areas for lapis lazuli were first described by Tosi and Piperno (1973). Ph. Colomban (2005) successively approached the use of lapis lazuli as a gem, as a pigment for maquillage, frescoes and ceramics and as a colourant for glass production. Provenance studies have been extensively debated but not solved (von Rosen 1988; Moorey 1999; Ballirano and Maras 2006; Zöldföldi *et al.* 2008; Smith and Klinshaw 2009). Most studies have focused on the Sar-e Sang deposits (Badakhshan province, Afghanistan) (see also Wyart *et al.* 1981; Faryad 2002; Aleksandrov and Senin 2006), rarely considering the close exploitable sources in Pakistan and Tajikistan (see, e.g., Casanova 1995).

With respect to the other gemstones, quartz and microcrystalline quartz have been less addressed in the archaeometric literature. Microcrystalline α-quartz and moganite were identified as the components of three engraved gemstones (Early Roman Empire period) found in central Paris (Smith and Robin 1997). Carnelians, sardonices, chalcedonies, jaspers, quartzes and agates from Crypta Balbi (Rome, Italy), worked between the end of Republican age and the seventh century AD, were further identified (Andreozzi *et al.* 1996), as well as quartz gems from the Guarrazar treasure (seventh century AD—Calligaro *et al.* 2000; Guerra *et al.* 2007). More attention has been paid to engraving techniques of hard gems such as quartz (Sax and Meeks 1995; Rosenfeld *et al.* 2003). The worldwide occurrence of quartz and chalcedony and their composition, frequently lacking in characteristic fingerprints (especially trace element content), deeply undermine the possibility of tracing their origin.

Three different methodologies have been approached so far in order to investigate the provenance of chalcedony and jasper. Insoll *et al.* (2004) applied the micro-destructive technique of laser-ablation inductively coupled plasma mass spectrometry (UV-LA–ICP–MS) to the study of a suite of major and trace elements and isotopes. The results did not allow a clear differentiation between Indian and sub-Saharan African carnelians, and the data shown are only

those obtained by statistical treatment (Principal Component Analysis). The second methodology involves non-destructive techniques such as proton-induced X-ray emission (PIXE) and proton-induced gamma-ray emission (PIGE) analyses, both applied by Theunissen *et al.* (2000) on carnelians from India and South-East Asia. The results provided chemical parameters for distinguishing carnelians of different origins, enabling a better understanding of the carnelian trade network. Based on Heaney and Post (1992), J. P. Pretola (2001) applied a third type of methodology using silica polymorph ratios, obtained by X-ray diffraction. The determination of the quartz:moganite ratio was presented as a 'promising approach' for the sourcing of chert and chalcedony.

Hence, in view of the quantity of materials investigated and the number of archaeological sites considered, the state of the art on gemstone studies is rather limited. On the contrary, the list of techniques used for gemstone characterization is rather long. Proton-induced X-ray emission (PIXE), sometimes combined with proton-induced gamma-ray emission (PIGE) or with Raman micro-spectrometry, has frequently been used (Xin Pei *et al.* 1993; Calligaro *et al.* 1998, 1999, 2000, 2001, 2002, 2006–7; Farges 1998; Yu *et al.* 2000; Guerra *et al.* 2007; Mathis *et al.* 2008). Portable PIXE-alpha and XRF spectrometers have been specifically tested on gems (Pappalardo *et al.* 2005). X-ray diffraction and X-ray fluorescence were employed for many decades, together with electron microprobe analyses and infrared spectroscopies (Andreozzi *et al.* 1996; Aurisicchio *et al.* 2006), while the Raman microprobe is being increasingly used (Bimson *et al.* 1982; Smith and Robin 1997; Hänni *et al.* 1998; Reiche *et al.* 2004). Photoluminescence spectroscopy proved to be a powerful tool when tested on commercial or synthesized samples, combined with Raman spectroscopy (Sodo *et al.* 2003). Lastly, oxygen isotopic composition provided a powerful but destructive method in tracing the origin of several gems (Giuliani *et al.* 2005).

MATERIALS AND METHODS

Given that (a) an accurate characterization of these gemstones, both in terms of chemical and mineralogical composition, was the issue of the present research, (b) the application of non-destructive techniques was mandatory, (c) XRD, Raman and PIXE analyses had been successfully applied for the mineralogical and chemical characterization of gemstones, and (d) only PIXE and XRD seemed to provide reliable results for quartz provenance investigations; we combined PIXE, Raman micro-spectroscopy and SR-XRD for the investigation of the gemstone collection.

To be precise, all of the chalcedonies were investigated by PIXE and SR-XRD, in order to determine their chemical composition, but especially to determine the quartz:moganite ratio. Given that the presence of certain mineralogical phases can provide a useful indication of lapis lazuli provenance, a detailed mineralogical composition was searched for through SR-XRD for this gemstone too. The remaining two samples (numbers 473572 and 473579) were mineralogically and chemically characterized by Raman micro-spectroscopy and PIXE, respectively.

Table 1 lists the 25 gemstones, providing information on their colour, diaphaneity (i.e., transparency), decoration, dimensions, find site and the analytical techniques used. Figure 1 shows the gemstone collection; in this regard, it is worth underlining that most of these gemstones are unpublished, therefore, better-resolution images could not be provided. The collection is currently under study by M. Rossi, who gave a preliminary illustration in the catalogue of the exhibition *Roma. Memorie dal sottosuolo. Ritrovamenti archeologici 1980/2006,* held in Rome in 2006–7 (Rossi 2007).

Table 1 *The gemstone list: dimensions are given as length × width × thickness*

Inventory no.	Diaphaneity	Colour	Decorations	Dimensions	Find site			SR-XRD	PIXE	Raman
					Area	Sector	Stratigraphic unit			
473213	Translucent	Colourless	Inscription	1.6 × 1.2 × 0.4	VB 92	A	4088-9	X	X	–
473581	Translucent	Colourless	Moon and seven stars (Pleiades)	1.3 × 1 × 0.4	VB 96	A	7758-1	X	X	–
473209	Translucent	Orange	Mars	1.2 × 0.9 × 0.2	VB 92	A	4088-5	X	–	–
473210	Translucent	Orange	Aesculapius	1.2 × 0.85 × 0.25	VB 92	A	4088-4	X	X	–
473214	Translucent	Orange	Victorious horse	1.15 × 0.9 × 0.2	VB 92	A	6576-1	X	–	–
473215	Translucent	Orange	Mars with sidus	1.6 × 0.9 × 0.2	VB 86	A	692-1	X	–	–
473575	Translucent	Orange	Standing figure	0.9 × 0.65 × 0.2	VB 96	A	7584-10	X	–	–
473576	Translucent	Orange	Mars	1 × 0.6 × 0.2	VB 96	A	7584-11	X	–	–
473578	Translucent	Orange	–	1.1 × 0.9 × 0.2	VB 96	A	7584-68	X	X	–
473584	Translucent	Orange	Ceres	1.2 × 1 × 0.15	VB 97	A	7815-28	X	–	–
473585	Translucent	Orange	Venus	1.45 × 1.1 × 0.2	VB 97	A	7815-37	X	X	–
473586	Translucent	Orange	Aesculapius	1.8 × 1 × 0.2	VB 97	A	7815-39	X	–	–
473568	Translucent	Orange with white coating	Male portrait	1.5 × 1.1 × 0.2	VB 92	B	1076-209	X	X	–
473216	Opaque	Orange	Shrimp	0.8 × 0.6 × 0.2	VB 96	A	7582-71	X	–	–
473573	Opaque	Orange	Parrot with cymbals in the mouth	0.9 × 0.7 × 0.1	VB 96	A	7582-71	X	X	–
473571	Translucent	Dark orange	Bull	1.85 × 1.5 × 0.25	VB 96	A	7582-26	X	X	–
473579	Transparent	Dark orange	Male profile surrounded by taenia	2 × 1.6 × 0.5	VB 96	A	7698-2	–	X	X
473569	Opaque	Blue	Agatodaimon (divinity with leonine head and snaky body) and inscription XNOYMIC on the back	1.25 × 0.85 × 0.2	VB 89	B	1142-64	X	X	–
473211	Opaque	Bluish black	Mars	1 × 0.7 × 0.2	VB 92	A	4088-6	X	X	–
473212	Opaque	Bluish black	Ant	0.9 × 0.7 × 0.2	VB 92	A	4088-7	X	X	–
473572	Transparent	Light green	–	0.85 × 0.65 × 0.2	VB 96	A	7582-28	–	X	X
473577	Translucent	Emerald green	Serapis portrait	1.1 × 0.8 × 0.2	VB 96	A	7584-15	X	X	–
473580	Translucent	Emerald green	Venus holding Mars' spear	1.3 × 0.9 × 0.1	VB 96	A	7722-1	X	X	–
473587	Translucent	Emerald green	Isis-Fortuna	1.2 × 0.85 × 0.25	VB 97	A	7815-40	X	–	–
473583	Opaque	Green with red spots	Sol	1.2 × 1 × 0.3	VB 97	A	7803-1018	X	X	–

Figure 1 *Gemstones from Vigna Barberini (Palatine Hill, Rome, Italy): the low resolution and the image dimensions cannot be improved, as this repertory is still under investigation.*

Synchrotron radiation X-ray diffraction (SR-XRD)

Given that the application of this technique represents a fundamental part of this research, the analytical procedure and, in the following paragraphs, the results obtained will be shown and discussed in great detail. X-ray diffraction (SR-XRD) patterns have been collected at the GILDA beamline (BM08; Meneghini *et al.* 2001) of the European Synchrotron Radiation Facility (ESRF-Grenoble), using an angle-dispersed set-up based on a large-area imaging plate (IP) detector (200×400 mm^2). A small X-ray spot size on the sample was obtained ($\sim 100 \times 100$ μm^2), focusing the X-ray beam with a couple of Pt mirrors (vertical) and sagittally bending the second monochromator crystal. The X-ray wavelength ($\lambda = 0.6151$ Å) and the geometrical parameters (the IP orientation and distance) were determined by refining the SR-XRD pattern of a LaB$_6$ (NIST) reference sample. In order to achieve the mineralogical characterization of 22 chalcedonies and jaspers and one likely lapis lazuli (sample 473569), 54 runs have been measured. In order to quantify the phase content, 50 diffractograms (excluding four of sample 473569) were analysed using the General Structure Analysis System (GSAS) program (Larson and Von Dreele 1986) for Rietveld refinement. Structural parameters at room temperature were taken from Gualtieri (2000) for quartz, Heaney and Post (2001) for moganite, Blake *et al.* (1966) for hematite and Szytula *et al.* (1968) for goethite, and not refined further. The refined parameters were as follows: the sample displacement, 19 parameters of a shifted Chebyshev background function, scale factors, peak profiles and the preferred orientation. The peak profile was modelled using a pseudo-Voigt function, refining both the Gaussian (GU, GW) and the Lorentzian (LY) coefficients, with a 0.01% cut-off of the peak. By enhancing the peak intensities of a certain class of reflections, the preferred orientation (i.e., the non-ideal or non-random distribution of the

crystalline orientation) was further refined. The March–Dollase correction (March 1932; Dollase 1986) was applied. The directions of the preferred orientation were determined by trial fittings, assuming the reflection indices of the otherwise poorly fitted profiles as the preferred orientation directions. The same refinement strategy was used for all data.

Micro-Raman spectroscopy

Spectra of samples 473572 and 473579 were recorded using a Jobin Yvon Ltd confocal Labram multichannel spectrometer, equipped with a Peltier-cooled charge-coupled device (CCD) detector and an Ar^+ laser ($\lambda = 514.5$ nm). The scattered light was analysed using a Notch holographic filter with a spectral resolution of 1.5 cm^{-1} and a grating of 1800 lines per millimetre. Calibration was performed using the 1332 cm^{-1} diamond band. Gemstones were placed under the microscope objective without any previous manipulation.

Proton-induced X-ray emission spectroscopy

PIXE measurements were performed at the 3 MV Tandetron accelerator of the INFN-LABEC laboratory (Laboratorio di tecniche nucleari applicate ai Beni Culturali; Mandò 2009) in Florence, using the external collimated beamline dedicated to applications in the field of cultural heritage. At the end of the beamline, the proton beam is extracted into the atmosphere from the vacuum line through a thin polymeric membrane (7.5 μm thick Upilex). The beam size is defined by collimation upstream of the beam exit window. The object under analysis is placed at a distance of about 1 cm from the beam exit window, on a target holder equipped with an *x*–*y* micrometric stage (plane perpendicular to the beam direction).

The PIXE detection system is based on two silicon detectors (Del Carmine *et al*. 1993) to collect X-rays emitted from the target irradiated with protons. The detectors are separately optimized for the detection of lower X-ray energies (1–8 keV, X-rays characteristic of low/medium-*Z* elements) and medium-to-high X-ray energies (4–30 keV, characteristic of heavier elements). On the whole, the system guarantees a high detection efficiency for the entire range of detectable elements (i.e., $Z \geq 11$, from sodium to the heaviest elements). For the analysis of the gemstones, we used the following detection conditions: (a) a silicon drift detector (SDD) by Ketek GmbH—with an energy resolution of 150 eV at 5.9 keV, a solid angle of approximately 4 msr, and a continuous He flow in front of the detector entrance window (8 μm thick Be), to enhance the transmission of low-energy X-rays; (b) a Si(Li) detector by Ortec—with an energy resolution of 185 eV at 5.9 keV, a solid angle of approximately 100 msr, and a 400 μm thick Mylar absorber in front of the detector, to eliminate the contribution of low-energy X-rays. For the gemstone analysis, we used a 2.9 MeV proton beam (energy on the target surface) with a diameter of about 0.5 mm. The beam current intensity was about 50 pA and the measuring time was 200–400 s for each analysed spot. The quantitative analysis of PIXE spectra was performed using the GUPIXWIN software (Maxwell *et al*. 1989, 1995). The quantity of oxygen (which is an 'invisible' element for external PIXE) has been calculated based on the charge balance (e.g., O bound as SiO_2 in chalcedony, SiO_4 for garnet and olivine etc.).

It is worthwhile stressing that the presence of non-homogeneities (e.g., different mineralogical phases) in the analysed volume (area of about 0.2 mm^2, thickness of the order of a few tens of micrometers) may alter the significance of the quantitative data; in this case, indeed, the composition measured by PIXE would be an average over the analysed volume. Under the experi-

mental conditions described, it was possible to characterize the elemental composition of the gemstones analysed, with quantification down to trace level (about 10–100 ppm) for most of the detected elements.

<div align="center">RESULTS</div>

The mineralogical characterization: synchrotron radiation X-ray diffraction (SR-XRD) and micro-Raman spectroscopy

The chalcedonies, the jaspers and the likely lapis lazuli (sample 473569) were investigated by SR-XRD, while samples 473572 and 473579 were characterized by micro-Raman spectroscopy. The 22 investigated chalcedonies and jaspers are constituted by variable proportions of quartz and moganite; weak peaks of hematite have been further observed in gemstones 473216 and 473573, and in the red spots of sample 473583, where goethite is present as well. Rietveld refinement techniques allowed for semi-quantitative determination of the crystalline phases present (Table 2). Most of the variability among the refinements may be due to compositional heterogeneity; however, the aberrations of the specimens (i.e., the displacement and transparency), the peak overlaps (i.e., the very similar quartz and moganite structures) and the broadening effects (crystallite size and microstrain problems) surely affect the goodness-of-fit. Peak broadening is marked in several histograms (see, for instance, the different broadening in patterns of gemstones 473216 and 473581 in Figs 2 (a) and 2 (b)). The microstrain (producing a Gaussian-shaped profile) and the crystallite size broadening (producing an intrinsic contribution to the Lorentz profile) may be due to different mountings and material heterogeneities (i.e., values vary considerably among different runs performed on a single specimen, especially for moganite). A marked preferential orientation further affects the accuracy of the quantitative estimations, although verifying the fibrous texture of the examined materials. In order to make this problem evident, each pattern in Figures 2 (a) – 2 (c) shows a series of arrows, located at different distances with respect to the tops of several peaks. Based on the intensity of the quartz peak at 3.34 Å (10-1), the tips of the arrows indicate where the intensity should rise/drop for the other quartz reflections; however, it is worth clarifying that the given examples start from the assumption (proven false for several runs) that the intensity of that quartz peak is correct. The quartz axes reported in Figures 2 (a) – 2 (c) are those creating the most problems, showing increased (March–Dollase parameter $r < 1$) or decreased ($r > 1$) intensities of reflections with an orientation near *hkl* (with $r = 1$ there is no preferred orientation). Although the displayed examples seem to show similar situations, it has been seen that data may vary from run to run, even if they are from the same sample. The χ^2 values may be indicative within this assemblage, as all refinements underwent exactly the same procedure. They ranged from 0.110 to 1.088 (with 80% of the values below 0.5), being higher for those refinements that deviated the most from their counterparts. Hence, the quantitative estimations—and especially the standard deviation values σ—cannot be taken at face value.

Given these necessary warnings, it is possible to explore the results. Based on gem type and colour (i.e., the principal *criteria* for the distinction of gem varieties), three scatter diagrams (quartz versus moganite) are provided in Figures 3 (a) – 3 (c). The first diagram (Fig. 3 (a)) plots values obtained for translucent orange gemstones, showing that the quartz:moganite ratio covers a wide range of values. Noticeable differences among orange chalcedonies can be found for specimens 473568 and 473575 (Fig. 2 (c)), respectively characterized by the highest and lowest contents of quartz (and vice versa for moganite). Quartz varies from 65 to 99 wt%; nevertheless,

Table 2 *Quantitative phase analyses on 22 gemstones, via the Rietveld method*

| Inventory no.	Run	χ^2	Phase fractions							
			Quartz		Moganite		Hematite		Goethite	
			wt%	σ	wt%	σ	wt%	σ	wt%	σ
473209	1	0.220	75.1	0.002	24.9	0.005				
	2	0.110	75.8	0.002	24.2	0.005				
	3	0.326	77.8	0.003	22.2	0.006				
	4	0.887	75.6	0.002	24.4	0.006				
473210	1	0.319	80.4	0.003	19.6	0.005				
473211	1	0.393	86.9	0.002	13.1	0.005				
	2	0.789	84.7	0.003	15.3	0.006				
473212	1	0.205	90.3	0.001	9.7	0.003				
	2	0.496	84.6	0.002	15.4	0.006				
473213	1	0.187	81.2	0.002	18.8	0.004				
	2	0.392	81.0	0.002	19.0	0.005				
473214	1	0.431	78.0	0.002	22.0	0.005				
	2	0.994	78.2	0.002	21.8	0.006				
	3	0.151	77.8	0.002	22.2	0.006				
	4	0.100	75.7	0.003	24.3	0.006				
473215	1	0.169	83.5	0.002	16.5	0.006				
	2	0.508	84.6	0.001	15.4	0.006				
473216	1	0.298	99.6	0.000	0.4	0.003				
	2	0.300	97.8	0.000	1.3	0.008	0.8	0.001		
473568	1	0.390	98.8	0.000	1.2	0.004				
473571	1	0.643	86.6	0.003	13.4	0.006				
473573	1	1.088	97.0	0.001	1.2	0.008	1.8	0.002		
473575	1	0.489	66.0	0.004	34.0	0.006				
	2	0.273	64.7	0.005	35.3	0.007				
473576	1	0.450	94.5	0.001	5.5	0.010				
	2	0.214	96.2	0.001	3.8	0.009				
473577	2	0.613	72.5	0.003	27.5	0.006				
	3	0.251	73.3	0.003	26.7	0.006				
	5	0.456	71.8	0.004	28.2	0.007				
473578	1	0.130	91.7	0.001	8.3	0.007				
	2	0.240	90.9	0.001	9.1	0.007				
473580	1	0.352	85.2	0.002	14.8	0.005				
	2	0.704	83.2	0.002	16.8	0.005				
	3	0.230	85.5	0.001	14.5	0.005				
	4	0.200	85.7	0.002	14.3	0.006				
473581	1	0.256	77.8	0.004	22.2	0.007				
	2	0.550	76.0	0.004	24.0	0.007				
473583	1	0.179	94.0	0.001	0.7	0.000	0.6	0.001	4.7	0.002
	2	0.310	92.4	0.001	0.7	0.002	1.6	0.002	5.3	0.002
473584	1	0.258	72.7	0.004	27.3	0.006				
	2	0.442	73.3	0.003	26.7	0.005				
473585	1	0.282	79.9	0.002	20.2	0.005				
473586	1	0.192	77.4	0.003	22.6	0.006				
	2	0.310	77.3	0.003	22.7	0.005				
473587	1	0.799	71.9	0.003	28.1	0.005				
	2	0.358	74.0	0.003	26.0	0.005				
	3	0.195	75.7	0.277	24.3	0.006				
	4	0.321	75.0	0.003	25.0	0.005				
	5	0.280	75.5	0.003	24.5	0.005				
	6	0.145	72.0	0.003	28.0	0.004				
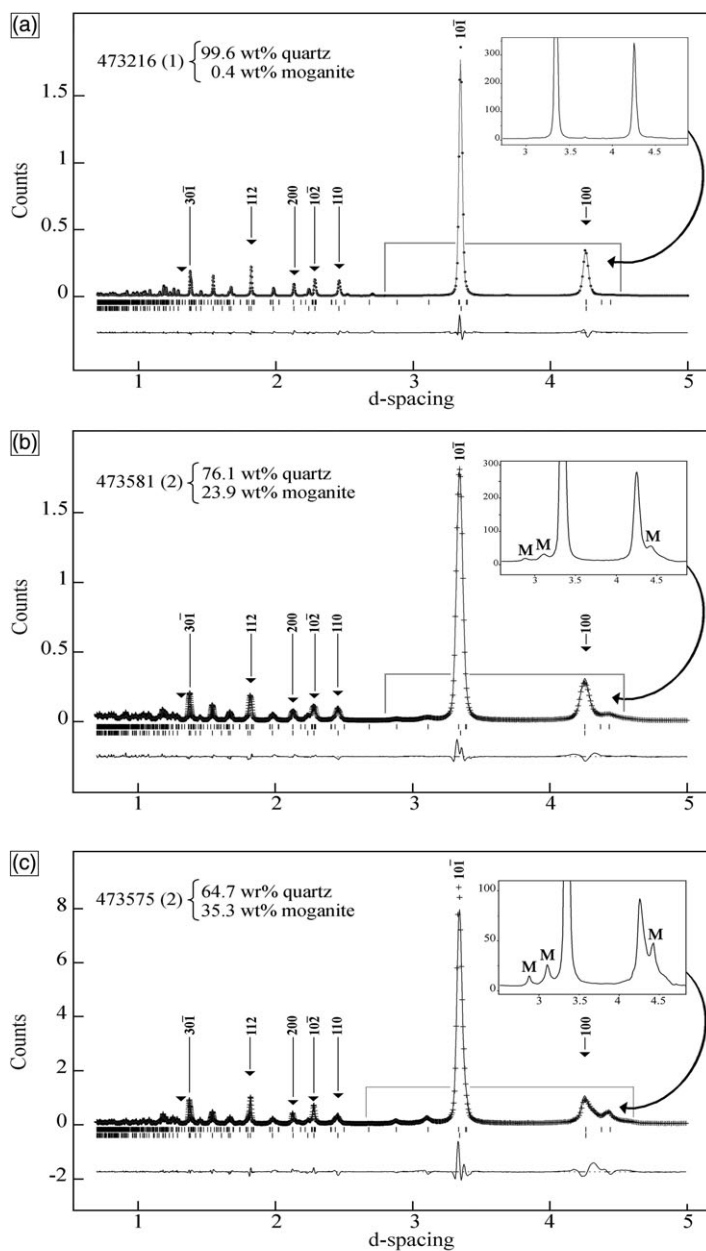
Figure 2   *Results obtained by SR-XRD. Diffraction patterns of gemstones: (a) 473216 (run 1); (b) 473581 (run 2); (c) 473575 (run 3). The enlarged view of the pattern between 2.6 and 4.8 Å is provided in boxes.*
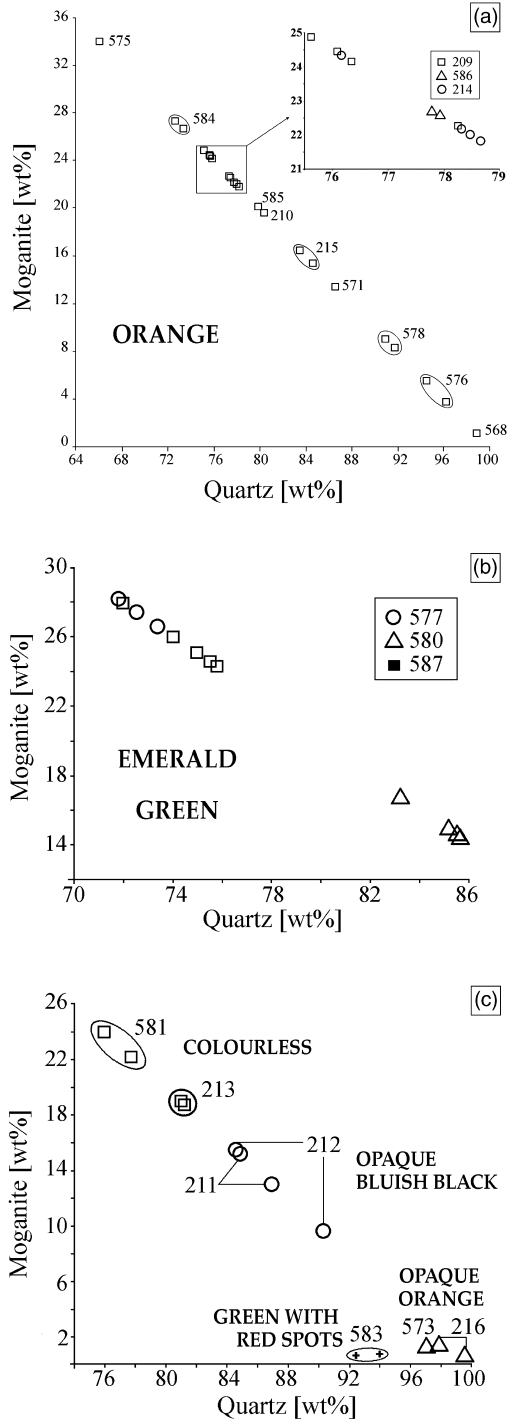
Figure 3   *Binary quartz–moganite diagrams for gemstones: (a) orange translucent; (b) emerald green; (c) colourless, bluish black, opaque orange and green with red spots.*
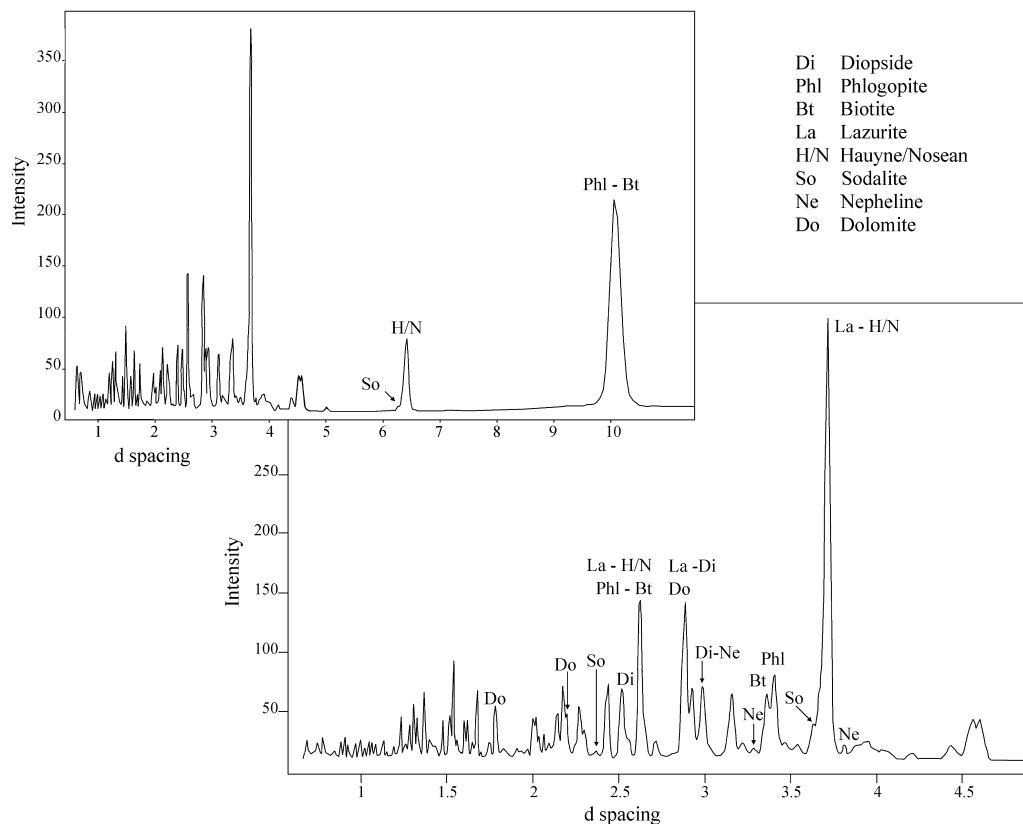
Figure 4 *Results obtained by SR-XRD. Diffraction patterns of lapis lazuli gemstone 473569.*

it is worth specifying precisely that: (a) the moganite peaks at 4.4 and 3.1 Å are not clearly visible in the diffractogram of specimen 473568, but Rietveld refinement accounts for 1.2 wt%; (b) moganite contents below 5 wt% (hence specimen 473576) cannot be fully resolved. The second diagram (Fig. 3 (b)) includes green gemstones, overlapping the composition of most orange ones. Specimens 473577 and 473587 show comparable quartz:moganite ratios, while specimen 473580 is slightly separated from the other two, being richer in quartz and poorer in moganite. Values for green gems vary between 72 and 86 wt% and between 14 and 28 wt% for quartz and moganite, respectively. The third diagram (Fig. 3 (c)) includes translucent colourless, opaque bluish black, opaque green with red spots and opaque orange gemstones. The quartz:moganite ratio is higher for the bluish black (5:1–9:1) than for the colourless variety (3:1–4:1). The moganite content is almost negligible in the opaque orange gemstone, as well as in the green one with red spots. In specimens 473216, 473573 and 473583, the hematite content (not shown) never exceeds 2 wt%. In specimen 473216, the presence of hematite in run no. 2 only should warn against considering hematite values as representative of the bulk composition. In specimen 473583, the goethite contents (~5 wt%) are higher than those of hematite. Lastly, the 23rd gemstone analysed by SR-XRD (sample 473569, Fig. 4) is constituted of lazurite, haüyne (/nosean), sodalite, diopside, phlogopite, biotite, dolomite and traces of nepheline. Given the typical mineralogical association of lapis lazuli, the presence of pyrite, calcite, sanidine and scapolite were further looked for, but were excluded.
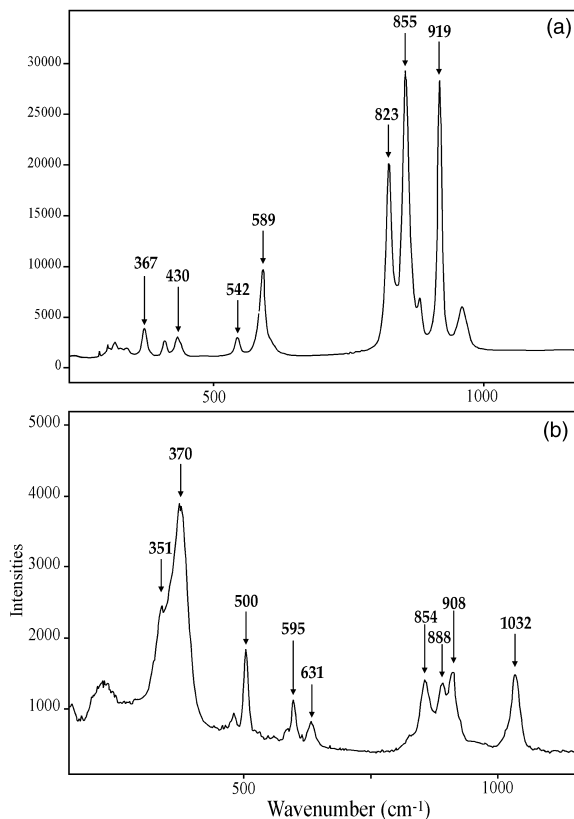
Figure 5 *Results obtained by Raman micro-spectroscopy: (a) spectrum of olivine gemstone 473572; (b) spectrum of almandine gemstone 473579.*

The micro-Raman spectra obtained for samples 473572 and 473579 characterized these gemstones as an olivine and a garnet, respectively. The spectra of gemstone 473572 (Fig. 5 (a)) are comparable to olivine $(Mg_{0.88}Fe_{0.12})_2SiO_4$ as reported in Chopelas (1991), rather than to the pure Mg end-member (forsterite; Mg_2SiO_4). Gemstone 473579 was identified as almandine (Fig. 5 (b)), the iron alumina garnet variety.

Proton-induced X-ray emission spectroscopy

The results of multi-elemental analyses performed on the quartz-based gemstones are provided in Table 3. Excluding run no. 3 of gemstone 473577, which has been performed on a dark inclusion, the SiO_2 content varies between 97.5 and 99.8 wt%. The Fe content is usually < 1 wt%, with the exception of gemstone 473573. Al, K and Ca are almost always present, but never exceeding 1 wt%. Mg, P and Cl have been sporadically measured, as well as Ti (in two gemstones only), that content of which is negligible (below 0.01 wt%). Trace contents of Ni, Cu, Zn and especially Pb have been detected in numerous quartz + moganite gemstones. The values obtained for run no. 3 of green gemstone 473577 have to be considered as the sum of quartz + moganite and a Cr- and Fe-bearing crystal inclusion (possibly a spinel), further containing small amounts

Table 3 *Chemical analyses performed by PIXE: concentrations are expressed as wt%; the uncertainty on the measured values is indicated in the cell immediately below the concentration*

Inventory no.	Run	SiO_2	Si	O	Mg	Al	P	Cl	K	Ca	Ti	Cr	Mn	Fe	Ni	Cu	Zn	Pb
473213	1	98.9	46.5	52.4		0.28	0.08	0.24	0.12	0.09				0.040				0.040
	±	1.20	0.6	2.5		0.04	0.03	0.02	0.02	0.01				0.010				0.020
473581	1	99.1	46.6	52.5	0.16	0.18	0.09	0.20	0.10	0.14				0.025		0.002		0.019
	±	0.29	0.1	0.6	0.04	0.04	0.03	0.02	0.02	0.01				0.002		0.001		0.005
473580	1	98.4	46.2	52.2		0.42		0.05	0.08	0.19		0.52		0.150	0.018	0.005		0.019
	±	0.27	0.1	0.6		0.03		0.01	0.01	0.01		0.05		0.010	0.002	0.001		0.004
	2	98.5	46.3	52.2		0.27			0.06	0.13		0.63		0.170	0.023			
	±	0.41	0.2	0.9		0.05			0.02	0.02		0.01		0.010	0.002			
473210	1	98.6	46.3	52.3		0.36			0.05	0.43				0.130				0.040
	±	0.39	0.2	0.8		0.05			0.02	0.02				0.040				0.010
473578	1	99.4	46.7	52.7		0.24	0.11	0.04	0.04	0.04				0.120				
	±	0.28	0.1	0.6		0.04	0.03	0.01	0.02	0.01				0.010				
	2	99.4	46.7	52.7		0.19			0.10	0.04				0.104				
	±	0.36	0.2	0.8		0.05			0.02	0.01				0.004				
473585	1	99.6	46.8	52.8		0.19			0.03	0.04				0.080				0.020
	±	0.27	0.3	0.6		0.04			0.01	0.01				0.003				0.010
	2	97.8	46.0	51.8		0.39	0.41	0.11	0.09	0.77			0.006	0.086		0.004		0.320
	±	0.33	0.2	0.7		0.04	0.05	0.02	0.02	0.02			0.002	0.004		0.001		0.020
	3	99.8	46.9	52.9		0.11			0.05					0.060				
	±	0.41	0.2	0.9														
473568	1	99.1	46.6	52.5		0.28	0.17			0.20				0.100		0.003	0.005	0.030
	±	0.33	0.2	0.7		0.04	0.04			0.02				0.010		0.001	0.001	0.060
	2	97.7	45.9	51.8		0.45		0.41	0.33	0.50				0.090		0.001	0.001	0.150
	±	0.29	0.1	0.6		0.04		0.03	0.02	0.02				0.004		0.001	0.001	0.010
	3	96.8	45.5	51.3		0.44	0.63	0.55	0.37	0.80				0.113		0.003	0.004	0.090
	±	0.32	0.2	0.7		0.04	0.05	0.03	0.03	0.03				0.000		0.001	0.001	0.008

Table 3 (Continued)

Inventory no.	Run	±	SiO₂	Si	O	Mg	Al	P	Cl	K	Ca	Ti	Cr	Mn	Fe	Ni	Cu	Zn	Pb
473573	1		97.5	45.8	51.7	0.28	0.17	0.09	0.04	0.03	0.14	0.01			1.300				
		±	0.27	0.1	0.6	0.05	0.04	0.03	0.01	0.01	0.01	0.01			0.020				
473571	1		98.4	46.2	52.2		0.14	0.77			0.50				0.034		0.004		0.022
		±	0.32	0.2	0.7		0.04	0.05			0.02				0.010		0.001		0.005
	2		99.4	46.7	52.7		0.15			0.04	0.10				0.026		0.002		0.005
		±	0.30	0.1	0.6		0.04			0.01	0.01				0.003		0.001		0.003
473211	1		99.6	46.8	52.8		0.11			0.03	0.08				0.003				0.011
		±	0.26	0.1	0.5		0.03			0.01	0.01				0.001				0.003
473212	1		99.4	46.7	52.7	0.12	0.16		0.05	0.08	0.09				0.005				0.007
		±	0.23	0.1	0.5	0.04	0.03		0.01	0.01	0.01				0.001				0.002
	2		99.5	46.8	52.7		0.18			0.10	0.07				0.005				0.002
		±	0.39	0.2	0.8		0.05			0.02	0.01				0.001				0.002
473577	1		99.1	46.6	52.5					0.05	0.10		0.28		0.160	0.008		0.009	0.030
		±	0.29	0.1	0.6					0.02	0.01		0.01		0.010	0.001		0.002	0.010
	2		99.1	46.6	52.5		0.18			0.05	0.12		0.22		0.130	0.006		0.007	0.070
		±	0.31	0.1	0.7		0.04			0.02	0.01		0.03		0.020	0.001		0.002	0.010
	3		81.3	38.2	43.1	0.36	0.69	0.35	0.09	0.06	0.35	0.09	10.7	0.17	4.900	0.025		0.050	0.440
		±	0.35	0.1	0.6	0.05	0.04	0.03	0.02	0.01	0.02	0.01	0.01	0.04	0.100	0.003		0.003	0.020
473583	1		97.8	46.0	51.8		0.27	0.08		0.25	0.63				0.560		0.004	0.003	0.018
		±	0.31	0.1	0.6		0.04	0.03		0.02	0.02				0.010		0.001	0.001	0.004

Notes: 473568, run no. 1 on the broken side of the gemstones, runs no. 2 and no. 3 on white coating; 473577, run no. 3 on inclusion.

of Mg and Mn. Cr is present in the translucent green gemstone 473580 as well. Figure 6 (a) shows the most relevant portions of the X-ray spectra obtained for specimen 473580, where the higher X-ray energy range reveals the presence of many medium-to-heavy elements (the main contribution of silicon could be seen from the other detector, whose spectrum is not displayed). Noticeable values of Al, K and Ca in run no. 2, and especially run no. 3, on the white coating of gemstone 473568 should indicate the presence of other mineralogical phases (e.g., calcium carbonate and feldspars), the contents of which are below the XRD detection limit. The Fe content is relatively high in opaque gemstones 473583 and especially 473573.

The results obtained for olivine (473572) and garnet (473579) gemstones are provided in Table 4, while the spectra are shown in Figures 6 (b) and 6 (c). Both gemstones show a rather stoichiometric composition. The olivine composition can be reported as $Fo_{79}Fa_{21}$ on average, containing further traces of Ni and Mn. Similarly, the garnet composition can be reported as $Al_{78}Gr_{17}Py_5$ on average, with traces of Mn ($Sp_{0.3}$). The lapis lazuli investigations revealed the presence of Si, Na, Mg, Al, S, K, Ca and Fe. This gemstone was only qualitatively investigated; X-ray diffraction identified a high number of different mineralogical phases, which were certainly simultaneously present in the volume analysed by PIXE. It is not straightforward to perform the quantitative analysis of such a heterogeneous sample (e.g., some elements can be attributed to different phases) and results would have very low significance. Figure 6 (d) shows the most relevant portions of the X-ray spectra obtained for this gemstone, characterized by lighter elements with Fe traces.

DISCUSSION

Calchedony and jasper

The gemstone colour can be used for naming the translucent orange varieties of chalcedony as carnelian, and the dark orange variety as sard, both coloured by iron inclusions. The translucent emerald green gemstones are chromium-bearing chalcedonies, with minor quantities of nickel. This variety is sometimes called matauralites or mtorolite. A Cr-bearing spinel (possibly detected in run no. 3 of gemstone 473577) should be responsible for the emerald green colour of this variety. Among the opaque gemstones, the orange ones are jaspers and the bluish-black ones are generally referred to as nicoli (or niccoli; i.e., onyx), while the green variety dotted with small, red, blood-like spots is heliotrope or bloodstone. Jasper and heliotrope are the only two varieties showing hematite and goethite in appreciable contents and very low amounts of moganite.

The PIXE measurements detected Cu, Pb and Zn in most chalcedonies. Research undertaken by Rosenfeld *et al*. (2003) demonstrated that these elements are frequently detected on gemstone surfaces, filling the engraved lines. Based on their study, lead and alumina can be related to lubrificants and abrasives, respectively; while Cu (and Zn) should be interpreted as residue of a rotating wheel/drill in bronze or brass.

Regarding carnelian specimen 473568, it is perhaps possible to hypothesize that a deliberate dying was performed, in order to whiten the gemstone. As reported by Rosenfeld *et al*. (2003), it was possible to achieve this effect by covering the gemstone with limestone ($CaCO_3$) and heating the whole to over 800°C, in order to favour the transformation of limestone into lime (CaO). Although heat treatment was a common practice (especially to enhance the colours of carnelians), the results obtained by the present research neither verify nor refute this hypothesis. On the other hand, the PIXE measurements showed that the coating layer contains more Al, K and Ca than the fresh gemstone, possibly supporting this hypothesis.
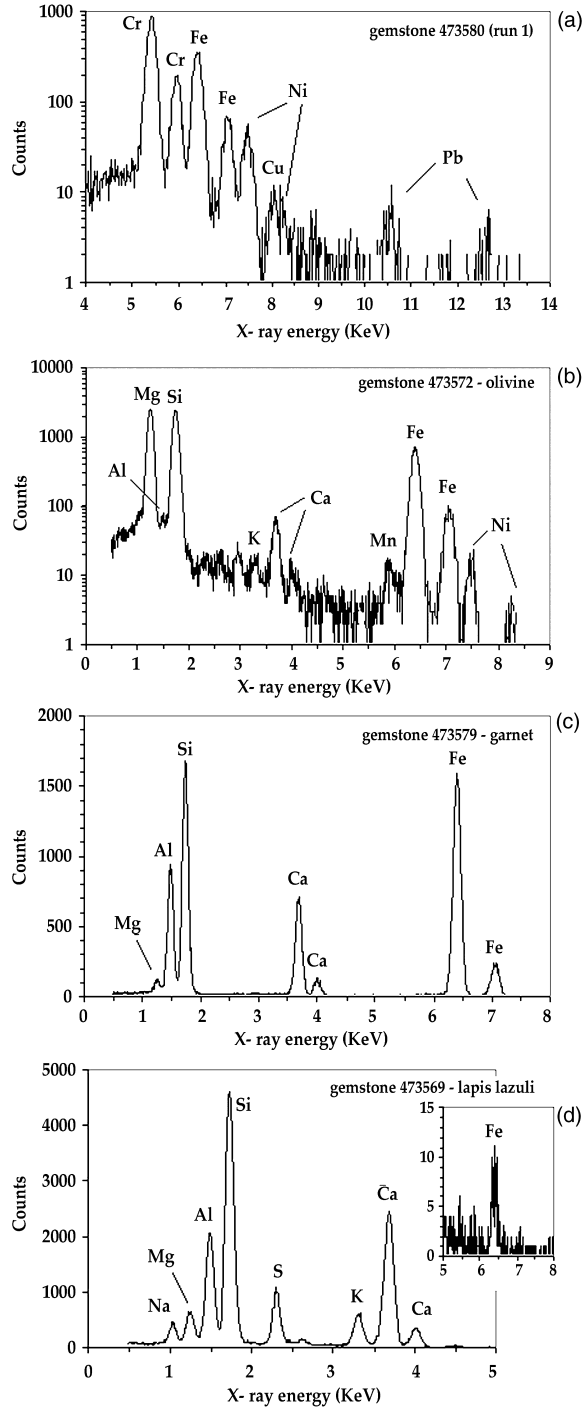
E. Gliozzo et al.

Figure 6   *Examples of PIXE spectra referring to the analysis of gemstones 473580, 473672, 473579 and 473569.*

Table 4   *Chemical analyses performed by PIXE: concentrations are expressed as wt%; the uncertainty of the measured values is indicated in the cell immediately below the concentration*

Inventory no.		SiO_4	Si	O	Mg	Al	Cl	K	Ca	Mn	Fe	Ni
473572	1	63.8	19.1	44.7	28.0	0.3	0.09	0.09	0.16	0.10	7.2	0.28
	±	1.10	0.2	2.0	0.3	0.1	0.03	0.02	0.02	0.01	0.5	0.02
	2	64.2	19.3	44.9	27.4	0.2	0.08	0.06	0.38	0.10	7.2	0.29
	±	0.68	0.1	1.2	0.2	0.1	0.02	0.01	0.02	0.01	0.2	0.02
473579	1	56.2	16.9	39.3	1.6	10.5	0.06		5.45	0.10	26.1	
	±	0.90	0.2	1.4	0.1	0.2	0.02		0.06	0.02	0.2	
	2	56.1	16.8	39.3	1.6	11.1			5.50	0.11	25.6	
	±	1.10	0.2	1.7	0.1	0.2			0.08	0.03	0.2	

Using silica polymorph ratios to source chalcedony, it is possible to hypothesize that a greatly different quartz:moganite ratio may indicate different origins. Although the limits of variability within a single source have not been specifically discussed in the available references, different origins are likely for gemstones 473216, 473568, 473573, 473576, 473583 and 473578, with a mean moganite content below 10 wt%, and gemstones 473577, 473584, 473587 and 473575, with a mean moganite content over 25 wt%. Considering that moganite has scarcely been found in altered rocks older than 150 Ma and that it is completely absent in rocks older than Devonian (Heaney 1995), it would be possible to direct searches towards outcrops younger than Devonian age; however, the possibilities still remain so numerous that the indication of a specific supply area should not be supported by the analytical data.

In fact, moganite is common in several geological conditions, its stability field is still uncertain (Heaney *et al*. 2007, and references therein) and its occurrence seems to be related both to the age (Devonian) and the surface weathering of the formation (Heaney and Post 1992, 2001; Heaney 1995; Gislason *et al*. 1997).

Using the PIXE results, the comparison with data provided by Theunissen *et al*. (2000) is compromised by the fact that the authors do not specify the error. However, it is possible to notice that chalcedonies from Vigna Barberini show Al, K, Ca and Fe contents that are consistently higher than those shown by the entire carnelian collection analysed by Theunissen *et al*. (2000); on the other hand, the Si values of our chalcedonies are generally comparable to those obtained for carnelians from India and Sri Lanka by the same authors. This evidence is not surprising. For instance, Pliny mentioned India among the areas supplying carnelians (*NH* 37.31.105–6) and India continues to supply the best carnelians up to the present day. Despite this intriguing coincidence, we must not ignore the fact that many other sources have been mentioned by ancient authors, and that mineralogical or chemical characterization is not available for further comparison. As an example, Pliny further mentioned Sardis (modern Sart), Babylon, Paros, Assos (modern Behramkal, Turkey), India, Arabia, Epirus, Egypt and an exhausted source in Persia for carnelian supply (*NH* 37.31.105–6); Amisos (modern Samsun, on the south coast of the Black Sea, Turkey), Chalcedon in Bithynia (modern Kadıköy, opposite Byzantium, south of Scutari) and India for the supply of green chalcedonies (*NH* 37.37.115); and Ethiopia, Africa and Cyprus for heliotrope supply (*NH* 37. 60.165).

Olivine, lapis lazuli and garnet

The gem quality form of forsteritic olivine is known as peridote, formerly called chrysolite. Gemstone 473569 is a lapis lazuli, constituted by a mixture of lazurite, haüyne (/nosean), sodalite, diopside, phlogopite, biotite, dolomite and traces of nepheline. Almandine is the main component of garnet gemstone 473579. The varieties comprised in the continuous series between almandine and pyrope are sometimes called rhodolite, even if the term is more frequently applied to a Mg-rich variety. Garnet, olivine and lapis lazuli did not show traces of Cu, Pb or Zn, suggesting a different engraving technique, as well as a different surface absorption, with respect to chalcedonies. In this regard, it is worth reminding that Pliny specified that peridote is the only gemstone affected by a file ('limam sentit'), whereas all the others have to be smoothed using an abrasive (stone of Naxos, possibly to be identified as emery) (NH 37.32.107–9). Lastly, it is worth noting that garnet was made more transparent by hollowing out the underside, following a practice already reported by Bauer (1968).

As far as provenance is concerned, the quaternary volcanic island of Saint John (Zabargad, Egypt), on the Egyptian coast of the Red Sea, about 80 km from Berenice harbour, is one of the best known sources for olivine (Wilson 1976); however, it is not possible to verify the validity of this or of many other hypotheses that can be equally made (e.g., Mogok in Myanmar or Soppat in Pakistan; for a complete list of sources, see, e.g., Rapp 2009). As for lapis lazuli, the mineralogical association of gemstone 473569 coincides with most known sources, such as those located in Afghanistan (Badakhshan, Sar-e Sang). The comprehensive studies made on scapolite-bearing rocks from the lapis lazuli deposit at Sar-e Sang by Faryad (2002), and on several of the world's lapis lazuli deposits by Aleksandrov and Senin (2006), help in tracing important similarities with the Afghan deposits. The evidence, however, is scarce, and the hypotheses that we would be able to formulate would depend greatly on other, better-known, cases (for further possible sources, see, e.g., Casanova 1995; Aleksandrov and Senin 2006).

As for garnet, the present results cannot be reasonably compared with those obtained by Calligaro *et al*. (2006–7). The garnet examined here is characterized by high FeO (32.9–33.6 wt %) and CaO (7.6–7.7 wt%) and low MgO (2.7 wt%); while the almandine garnets included in Types I and II by Calligaro *et al*. (2006–7) are both characterized by high FeO (32.1–37.5 wt%), but lower CaO (0.7–1.4 wt%) and higher MgO (4.4–6.2 wt%) contents.

CONCLUSIONS

The combination of SR-XRD, Raman micro-spectroscopy and PIXE analytical techniques proved to be particularly effective in order to obtain a complete, accurate, non-destructive and non-invasive characterization of the gemstones. The collection from Vigna Barberini consists of 20 chalcedonies (two colourless, 11 carnelians, one sard, three Cr-bearing chalcedonies, two nicoli and one heliotrope), two orange jaspers, one almandine garnet, one peridote and one lapis lazuli. The provenance issues are greatly complicated by the worldwide occurrence of all these gemstones. The measurement of silica polymorphs and the determination of chemical composition by PIXE do not provide sufficient information in order to reconstruct preferential routes for gemstone trade; however, the exploitability of these results is largely affected by the scarcity of reference data with which to compare. For this reason, we believe that the obtained data can help create the discriminant parameters for provenance investigation. In fact, with regard to the future perspective of a database specifically created for chalcedonies, we could face a long and fruitless wait.

Nevertheless, the distinction between the place of extraction and the place of manufacture has always to be made. It is well known that, in Roman times, businesses could cover surprising distances, especially when the object being marketed was a precious, lightweight and not bulky material; on the other hand, manufacture must include experienced artisans, responsible for cutting and engraving techniques, in order to satisfy sociocultural requirements (mainly fashion and superstition). It is thus straightforward that the places of extraction do not necessarily coincide with the place of manufacture.

REFERENCES

Aleksandrov, S. M., and Senin, V. G., 2006, Genesis and composition of lazurite in magnesian skarns, *Geochemistry International*, **44**, 976–88.

Andreozzi, G. B., Graziani, G., and Saguì, L., 1996, Gems from archaeological excavations at Rome (Cripta Balbi), *Zeitschrift der Deutschen Gemmologischen Gesellschaft*, **4**, 49–72.

Aurisicchio, C., Corami, A., Ehrman, S., Graziani, G., and Nunziante Cesaro, S., 2006, The emerald and gold necklace from Oplontis, Vesuvian Area, Naples, Italy, *Journal of Archaeological Science*, **33**, 725–34.

Ballirano, P., and Maras, A., 2006, Mineralogical characterization of the blue pigment of Michelangelo's fresco 'The Last Judgment', *American Mineralogist*, **91**, 997–1005.

Bauer, M., 1968, *Precious stones*, Dover Publications, New York.

Bimson, M., La Niece, S., and Leese, M. N., 1982, The characterization of mounted garnets, *Archaeometry*, **24**, 51–8.

Blake, R. L., Hessevick, R. E., Zoltai, T., and Finger, L. W., 1966, Refinement of the hematite structure, *American Mineralogist*, **51**, 123–9.

Calligaro, T., Poirot, J.-P., and Querré, G., 1999, Trace element fingerprinting of jewellery rubies by external beam PIXE, *Nuclear Instruments and Methods in Physics Research B*, **150**, 628–34.

Calligaro, T., Colinart, S., Poirot, J.-P., and Sudres, C., 2002, Combined external-beam PIXE and μ-Raman characterisation of garnets in Merovingian jewellery, *Nuclear Instruments and Methods*, **B189**, 320–7.

Calligaro, T., Dran, J.-C., Poirot, J.-P., and Querré, G., 2001, Ion beam analysis techniques: a powerful set of tools for the identification and sourcing of ancient gems, in *Proceedings of III Congreso Nacional de Arqueaometría* (eds. B. M. G. Tubío, M. A. Respaldiza and M. L. P. Rodríguez), 197–206, Secretariado de Publicaciones, Sevilla.

Calligaro, T., Mossmann, A., Poirot, J.-P., and Querré, G., 1998, Provenance study of rubies from a Parthian statuette by PIXE analysis, *Nuclear Instruments and Methods in Physics Research B*, **136–8**, 846–50.

Calligaro, T., Perin, P., Vallet, F., and Poirot, J.-P., 2006–7, Contribution à l'étude des grenats mérovingiens (Basilique de Saint-Denis et autres collections du musée d'Archéologie nationale, diverses collections publiques et objets de fouilles récentes). Nouvelles analyses gemmologiques et géochimiques effectuées au Centre de recherche et de Restauration des Musées de France, *Antiquités Nationales*, **38**, 111–44.

Calligaro, T., Dran, J.-C., Poirot, J.-P., Querré, G., Salomon, J., and Zwaan, J. C., 2000, PIXE/PIGE characterisation of emeralds using an external micro-beam, *Nuclear Instruments and Methods in Physics Research B*, **161–3**, 769–74.

Casanova, M., 1995, Le lapis-lazuli dans l'Orient antique, in *Les pierres précieuses de l'Orient ancien des Sumériens aux Sassanides. Exposition-dossier du Département des Antiquités Orientales, Musée de Louvre* (ed. F. Tallon), 15–20, Réunion des musées nationaux, Paris.

Chopelas, A., 1991, Single crystal Raman spectra of forsterite, fayalite, and monticellite, *American Mineralogist*, **76**, 1101–9.

Colomban, Ph., 2005, Routes du lapis lazuli, lâjvardina et échanges entre arts du verre, de la céramique et du livre, in *Chine-Méditerranée, routes et échanges de la céramique avant le XVIè siècle*, 145–52, *Taoci* 4, Editions Findakly.

Del Carmine, P., Lucarelli, F., Mandò, P. A., and Pecchioli, A., 1993, The external PIXE setup for the analysis of manuscripts at the Florence University, *Nuclear Instruments and Methods in Physics Research B*, **75**, 480–4.

Dollase, W. A., 1986, Correction of intensities for preferred orientation in powder diffractometry: application of the March model, *Journal of Applied Crystallography*, **19**, 267–72.

Farges, F., 1998, Mineralogy of the Louvre's Merovingian garnet cloisonné jewelry: origins of the gems of the first kings of France, *American Mineralogist*, **83**, 323–30.

Faryad, S. W., 2002, Metamorphic conditions and fluid compositions of scapolite-bearing rocks from the lapis lazuli deposit at Sare Sang, Afghanistan, *Journal of Petrology*, **43**, 725–47.

Gislason, S. R., Heaney, P. J., Oelkers, E. H., and Schott, J., 1997, Kinetic and thermodynamic properties of moganite, a novel silica polymorph, *Geochimica Cosmochimica Acta*, **61**, 1193–204.

Giuliani, G., Fallick, A. E., Garnier, V., France-Lanord, C., Ohnenstetter, D., and Schwarz, D., 2005, Oxygen isotope composition as a tracer for the origins of rubies and sapphires, *Geology*, **33**, 249–52.

Gualtieri, A. F., 2000, Accuracy of XRPD QPA using the combined Rietveld–RIR method, *Journal of Applied Crystallography*, **33**, 267–78.

Guerra, M. F., Calligaro, T., and Perea, A., 2007, The treasure of Guarrazar: tracing the gold supplies in the Visigothic Iberian peninsula, *Archaeometry*, **49**, 53–74.

Hänni, H. A., Schubiger, B., Kiefert, L., and Häberli, S., 1998, Raman investigations on two historical objects from Basel Cathedral: the Reliquary cross and Dorothy monstrance, *Gems & Gemology*, **34**, 102–25.

Heaney, P. J., 1995, Moganite as an indicator for vanished evaporites: a testament reborn? *Journal of Sedimentary Research*, **A65**, 633–8.

Heaney, P. J., and Post, J. E., 1992, The widespread distribution of a novel silica polymorph in microcrystalline quartz varieties, *Science*, **255**, 441–3.

Heaney, P. J., and Post, J. E., 2001, Evidence for an I2/a to Imab phase transition in the silica polymorph moganite at ~570 K, *American Mineralogist*, **86**, 1358–66.

Heaney, P. J., McKeown, D. A., and Post, J. E., 2007, Anomalous behavior at the I2/a to Imab phase transition in SiO_2-moganite: an analysis using hard-mode Raman spectroscopy, *American Mineralogist*, **92**, 631–9.

Insoll, T., Polya, D. A., Bhan, K., Irving, D., and Jarvis, K., 2004, Towards an understanding of the carnelian bead trade from western India to sub-Saharan Africa: the application of UV-LA–ICP–MS to carnelian from Gujarat, India, and West Africa, *Journal of Archaeological Science*, **31**, 1161–73.

Larson, A. C., and Von Dreele, R. B., 1986, *General structure analysis system*, Report LA-UR-86-748, Los Alamos National Laboratory, Los Alamos, NM.

Mandò, P. A., 2009, INFN-LABEC—Nuclear techniques for cultural heritage and environmental applications, *Nuclear Physics News*, **19**, 5–12.

March, A., 1932, Mathematische Theorie der Regelung nach der Korngestalt bei affiner Deformation, *Zeitschrift für Kristallographie*, **81**, 285–297.

Mathis, F., Vrielynck, O., Laclavetine, K., Chêne, G., and Strivay, D., 2008, Study of the provenance of Belgian Merovingian garnets by PIXE at IPNAS cyclotron, *Nuclear Instruments and Methods in Physics Research B*, **266**, 2348–52.

Maxwell, J. A., Campbell, J. L., and Teesdale, W. J., 1989, The Guelph PIXE software package, *Nuclear Instruments and Methods in Physics Research B*, **43**, 218–30.

Maxwell, J. A., Teesdale, W. J., and Campbell, J. L., 1995, The Guelph PIXE software package II, *Nuclear Instruments and Methods in Physics Research B*, **95**, 407–21.

Meneghini, C., Artioli, G., Norby, P., Balerna, A., Gualtieri, A., and Mobilio, S., 2001, Translating image plate system for *in-situ* experiments at GILDA beamline, *Journal of Synchrotron Radiation*, **8**, 1162–6.

Moorey, P. R. S., 1999, *Ancient Mesopotamian materials and industries: the archaeological evidence*, Eisenbrauns, Winona Lake, IN.

Pappalardo, L., Karydas, A. G., Kotzamani, N., Pappalardo, G., Romano, F. P., and Zarkadas, Ch., 2005, Complementary use of PIXE-alpha and XRF portable systems for the non-destructive and *in situ* characterization of gemstones in museums, *Nuclear Instruments and Methods in Physics Research B*, **239**, 114–21.

Pretola, J. P., 2001, A feasibility study using silica polymorph ratios for sourcing chert and chalcedony lithic materials, *Journal of Archaeological Science*, **28**, 721–39.

Rapp, G., 2009, *Archaeomineralogy*, Springer-Verlag, Berlin.

Reiche, I., Pagès-Camagna, S., and Lambacher, L., 2004, *In situ* Raman spectroscopic investigations of the adorning gemstones on the reliquary *Heinrich's Cross* from the treasury of Basel Cathedral, *Journal of Raman Spectroscopy*, **35**, 719–25.

Rosenfeld, A., Dvorachek, M., and Amorai-Stark, S., 2003, Roman wheel-cut engraving, dyeing and painting micro-quartz gemstones, *Journal of Archaeological Science*, **30**, 227–38.

Rossi, M., 2007, 1.18—Gruppo di ventotto gemme, in *Roma. Memorie dal sottosuolo. Ritrovamenti archeologici 1980/2006* (Roma, Oleare Papali alle Terme di Diocleziano, 2 Dicembre 2006–9 Aprile 2007) (ed. M. A. Tomei), 63.

Sax, M., and Meeks, N. D., 1995, Methods of engraving quartz cylinder seals, *Archaeometry*, **37**, 25–36.

Smith, D. C., and Robin, S., 1997, Early Roman Empire intaglios from 'rescue excavations' in Paris: an application of the Raman microprobe to the non-destructive characterization of archaeological objects, *Journal of Raman Spectroscopy*, **28**, 189–93.

Smith, G. D., and Klinshaw, R. J. II, 2009, The presence of trapped carbon dioxide in lapis lazuli and its potential use in geo-sourcing natural ultramarine pigment, *Journal of Cultural Heritage*, **10**, 415–21.

Sodo, A., Nardone, M., Ajò, D., Pozza, G., and Bicchieri, M., 2003, Optical and structural properties of gemmological materials used in works of art and handicraft, *Journal of Cultural Heritage*, **4**, 317–20.

Szytula, A., Burewicz, A., Dimitrijevic, Z., Krasnicki, S., Rzany, H., Todorovic, J., Wanic, A., and Wolski, W., 1968, Neutron diffraction studies of alpha-FeOOH, *Physica Status Solidi B*, **26**, 429–34.

Theunissen, R., Grave, P., and Bailey, G., 2000, Doubts on diffusion: challenging the assumed Indian origin of Iron Age agate and carnelian beads in Southeast Asia, *World Archaeology*, **32**, 84–105.

Tosi, M., and Piperno, M., 1973, Lithic technology behind the ancient lapis lazuli trade, *Expedition*, **16**, 15–23.

Villedieu, F., 2001, *Il giardino dei Cesari. Dai palazzi antichi alla Vigna Barberini, sul Monte Palatino. Scavi dell'École française de Rome 1985–1999*, Quasar, Roma.

Villedieu, F., 2007, La Vigna Barberini sul Palatino, in *Roma. Memorie dal sottosuolo. Ritrovamenti archeologici 1980/2006* (Roma, Oleare Papali alle Terme di Diocleziano, 2 Dicembre 2006–9 Aprile 2007) (ed. M. A. Tomei), 56–9.

von Rosen, L., 1988, *Lapis lazuli in geological contexts and in ancient written sources*, Paul Ånströms Förlag, Gothenberg, Sweden.

Wilson, W., 1976, Famous mineral localities: Saint John's Island, Egypt, *Mineralogical Record*, **7**, 310–14.

Wyart, J., Bariand, P., and Filippi, J., 1981, Lapis-lazuli from Sar-e-Sang, Badakhshan, Afghanistan, *Gems & Gemmology*, **17**, 184–90.

Xin Pei, M., MacArthur, J. D., Roeder, P. L., and Mariano, A. N., 1993, Trace element fingerprinting of emeralds by PIXE/PIGE, *Nuclear Instruments and Methods in Physics Research B*, **B75**, 423–7.

Yu, K. N., Tang, T. S., and Tay, T. S., 2000, Nuclear microscopic studies of inclusions in natural and synthetic emeralds, *X-ray Spectrometry*, **29**, 178–86.

Zöldföldi, J., Richter, S., Kasztovszky, Z., and Mihály, J., 2008, Where does lapis lazuli come from? Non-destructive provenance analysis by PGAA, in *Proceedings of the 34th International Symposium on Archaeometry (Zaragoza, Spain, May 3–7, 2004)* (ed. J. Pérez-Arantegui), 353–61.